A Method to Evaluate Nonideal Effects of Anechoic Chambers for Multiple-Angle Measurements

Michael H. Denison

A capstone project report submitted to the faculty of
Brigham Young University
in partial fulfillment of the requirements for the degree of

Bachelor of Science

Timothy W. Leishman, Advisor

Department of Physics and Astronomy

Brigham Young University

25 April 2016

ABSTRACT

A Method to Evaluate Nonideal Effects of Anechoic Chambers for Multiple-Angle Measurements

Michael H. Denison
Department of Physics and Astronomy, BYU
Bachelor of Science

Anechoic chambers are typically qualified by comparing sound pressures at several radial distances from a sound source and verifying that they follow the spherical spreading law within specified tolerances. While this technique is useful, it may not sufficiently characterize free-field variations at fixed radial distances and numerous angular positions, as are commonly used for directivity, sound power, and other important acoustical measurements. This paper discusses a technique to detect angular field deviations in anechoic chambers. It incorporates a loudspeaker in an altazimuth mount, an adjustable-radius boom arm, and a precision microphone. The boom arm and microphone remain in line with the loudspeaker driver axis at a fixed radius while the system rotates to specified azimuthal angle increments. In an ideal free-field environment, the frequency-response function from the loudspeaker input signal to the microphone output signal should remain consistent—regardless of the system orientation. However, in typical anechoic chambers, they vary. Standard deviation calculations over many angles reveal frequency-dependent departures from the ideal, especially for narrow-band data. The results show the impact of these discrepancies for multiple-angle measurements and how they change with radial distance from the source.

Keywords: anechoic chamber, room modes

ACKNOWLEDGEMENTS

First and foremost, I thank my wife Alisha for supporting me through the late nights in the chamber, being an involved editor of this report, and creating a peaceful home environment where I could relax and work.

I thank Joshua Bodon for developing data acquisition techniques and the fundamentals for the data analysis used in this research.

I thank Dr. Timothy Leishman for his continual insight and direction.

A special thanks to the BYU physics and astronomy department for funding much of this capstone work.

I also thank all of the undergraduate researchers that helped along the way, especially Adam Erickson and Konrie Ming who have made significant contributions in collecting data.

Table of Contents

List of Figures

Chapter 1

Introduction

Anechoic chambers have been vital in many areas of acoustical research for the past several decades. The purpose of an anechoic chamber is to produce a free-field environment, or an environment wherein there are no appreciable sound reflections within the frequency range of interest. A suitably performing anechoic chamber is crucial for acquiring reliable acoustical data. Nonideal field effects of an anechoic chamber will result in an unexpected spatial dependence of acoustical response. This paper develops a new approach for evaluating the field characteristics in anechoic chambers and shows the resulting spatial dependence of acoustical response for a specific chamber. The methods described in this paper may be used in future research to provide more rigorous qualification standards for anechoic chambers.

1.1 Background

Anechoic chambers need to be qualified before they can be used for research. According to international standard ISO 3745:2012 [1], they are qualified if radial measurements follow the inverse-square law within a certain tolerance. This is done by making a minimum of five linear traverse measurements away from an omnidirectional source. For each measurement, sound

pressure recordings are taken at either continuous or discrete increments. After at least 50 recordings are made, the measurements are compared to the inverse-square law. The chamber is considered "anechoic" if the one-third-octave band frequencies of the measurements follow the inverse-square law within the tolerances specified in Table 1.

Although linear traverses provide a simple way to qualify chambers, they do not accurately characterize many common forms of measurements performed in them. It is more common that researchers want to understand the sound field surrounding a source rather than at increasing distances at a specified radiation angle. This is typically done by taking multiple-angle measurements at a fixed or nearly fixed radius, as is common in directivity and sound power measurements. It is important that variations in the multiple-angle measurements are characteristics of the sound source and not artifacts caused by the chamber. For a truly omnidirectional source, the sound field should be identical at any angle of fixed radius in a free-field environment. Deviations in fixed-radius, multiple-angle measurements that are caused by the chamber would not be adequately characterized using linear traverses.

Studies have shown limitations to the current ISO standard for qualifying anechoic chambers. The standard allows for the omnidirectional source to produce either a broadband or a

Table 1. Allowable deviations for linear-traverse measurements in the anechoic chamber qualification described in ISO 3745:2012.

One-third-octave band frequency (Hz)	Allowable deviation (dB)
≤ 630	± 1.5
800 to 5000	± 1.0
≥ 6300	± 1.5

pure-tone test signal. Cunefare and others have found that there is a significant difference in the inverse-square law deviations depending on the chosen test signal [2] [3] [4]. Another issue with the current standard is that it requires a special omnidirectional loudspeaker [5]. These can be expensive to purchase and difficult to make. An alternate method of qualifying an anechoic chamber would be useful for researchers who do not have this resource.

Research at other institutions has shown imperfections in anechoic chambers due to areas with hard surfaces, such as lights or floor panels [6]. Others have found variances in chambers due to vibrations in the walls [7]. Although it is important to understand these imperfections, it is currently difficult to determine the extent these imperfections might have on fixed-radius, multiple-angle measurements.

It is well known that every anechoic chamber has a low-frequency cutoff, or a frequency below which the chamber cannot ideally absorb sound. It is typical for researchers to limit their analyses to frequencies above this frequency. Any nonanechoic or nonideal effects of the chamber field are generally ignored at higher frequencies.

1.2 Motivations

Current Brigham Young University research in musical instrument directivity uses an anechoic chamber for its nearly free-field environment. Bodon [8] has produced narrow-band, high-resolution directivity balloon plots for many musical instruments and loudspeakers. In many of these plots, he has seen several strange latitudinal bands or ridges in the results. Figure 1 shows the measurement configuration for a Tannoy System 800 loudspeaker and Fig. 2 shows the resulting directivity balloon plots at 1.8 kHz (note that 1.8 kHz is well above the low-frequency cutoff of the chamber used). Figure 2(a) shows the bands most prominently between

the orange and yellow regions. Figure 2(b) shows the bands most prominently in the jagged edges on the bottom-right of the plot. Bodon has ensured that these bands are not a characteristic of the loudspeaker, nor a result of errors in data acquisition, but are potentially caused by imperfections in the anechoic chamber. Knowing the cause of these bands would greatly increase the credibility of the work done by Bodon and the BYU directivity measurement system.

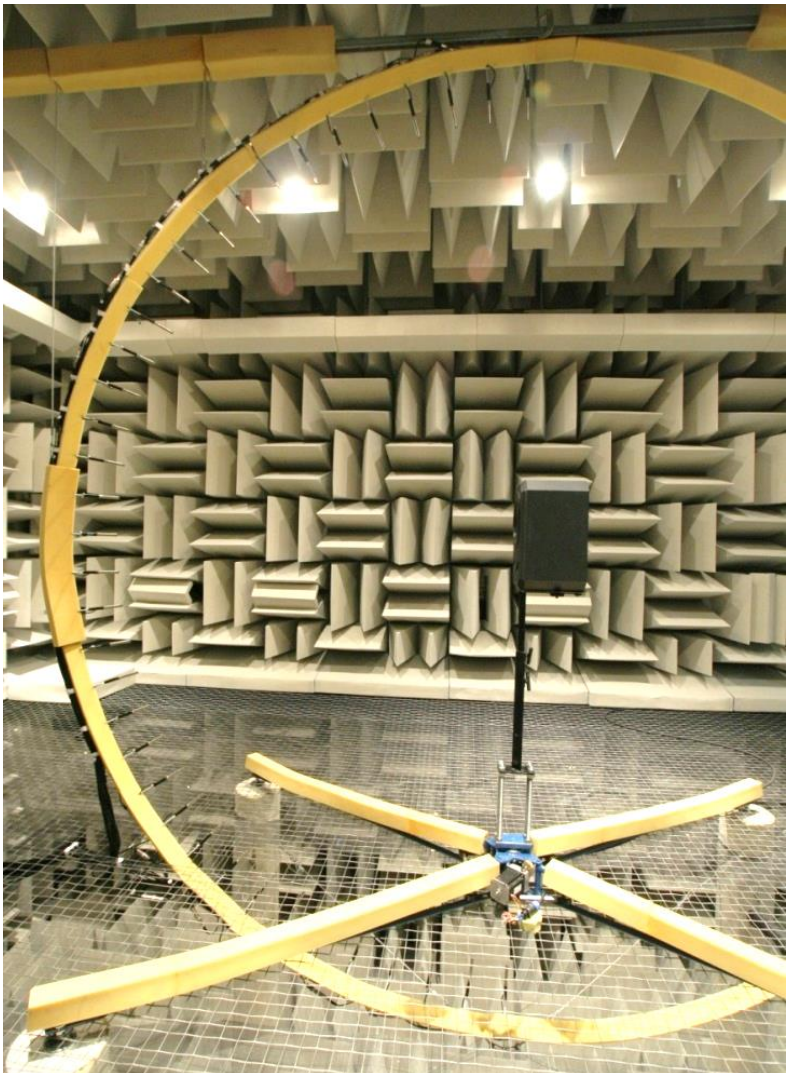

Figure 1. The BYU directivity measurement system with the Tannoy System 800 loudspeaker.

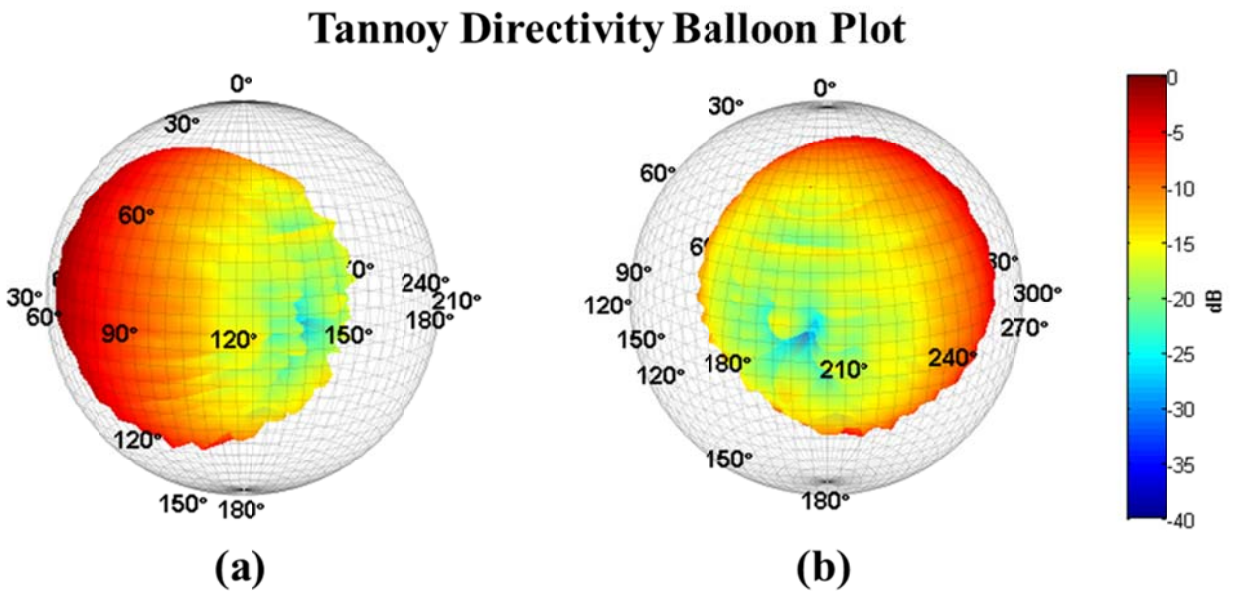

Figure 2. Directivity of a Tannoy System 800 loudspeaker at 1.8 kHz with horizontal bands from Bodon's research [8]. (a) Left-rear view of the directivity balloon. (b) Right-rear view of the directivity balloon.

1.3 Objectives

This paper addresses the question of whether or not an anechoic chamber could be a significant source of error in fixed-radius, multiple-angle measurements such as directivity and sound power measurements. Understanding the chamber's effects on these types of measurements will allow future researchers to better characterize sound sources. This project pioneers a new method of testing the free-field response of anechoic chambers that will more accurately detect spatial deviations in the sound field. This is done by implementing an experimental constant-excitation device that will perform fixed-radius, multiple-angle measurements. Standard deviation and frequency response function analysis shows the extent of spatial deviations in the anechoic chamber.

The chamber that will be discussed in this report is the BYU anechoic chamber. It has working dimensions of 8.71 × 5.66 × 5.74 m and an anechoic range from approximately 80 Hz to 20 kHz.

Chapter 2

Methods

As shown in Fig. 3, the experimental constant-excitation device is a loudspeaker and microphone rotation system in which the loudspeaker is attached to a mount that is connected to a turntable that rotates to discrete azimuthal angles. An acoustically treated boom arm is attached with a microphone at the end that keeps the microphone on the principal axis of the loudspeaker while the loudspeaker is rotated by the turntable. This ensures that the loudspeaker, boom arm and microphone are always in the same reference frame regardless of loudspeaker orientation. If the reference frame is not maintained, the changing scattering surfaces of the boom arm and directivity characteristics of the loudspeaker and of the microphone could affect the data. The mount is capable of adjusting the inclination angle of the loudspeaker and boom arm, but this feature was not used in this study.

The microphone boom arm may be adjusted to alter the radial distance between the microphone and loudspeaker. This expands the amount of usable data that the constant-excitation device can capture. At closer distances, the microphone will detect sound dominated more strongly by the direct field of the loudspeaker. At farther distances, nonanechoic effects of the chamber will be more apparent.

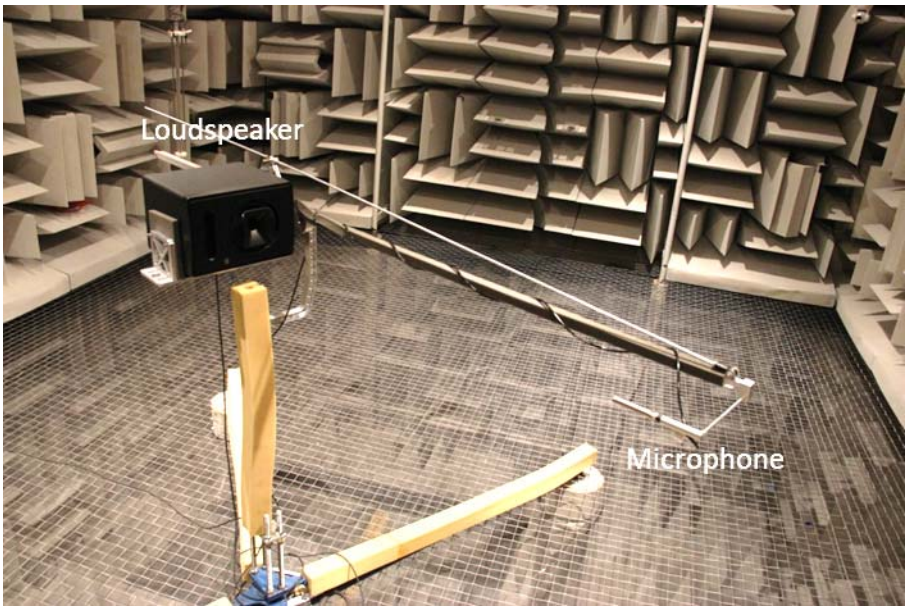

Figure 3. The experimental constant-excitation device that uses a loudspeaker on an altazimuth mount and a microphone on a boom arm in the BYU anechoic chamber.

The loudspeaker used in this research was a PreSonus Sceptre S6 coaxial loudspeaker. A coaxial loudspeaker is advantageous over a traditional 2-way loudspeaker to avoid radiation nulls near the crossover frequency. The microphone used was a GRAS 40AE ½ inch type-1 microphone paired with a Larson Davis PRM 426 microphone preamplifier. A Focusrite RedNet 4 digital audio interface and REAPER digital audio workstation were used to record the data.

At each measurement location, the loudspeaker generated 30 s of Gaussian noise. The first 10 s were used to excite the room. The latter 20 s were used to calculate frequency response functions (FRFs) for each measurement location. The FRFs were calculated with reference to the digital form of the input signal to the loudspeaker with 37, 1 s averages and 50% overlap. After the recording was completed, the loudspeaker and microphone were rotated by 5^{o}. Because of the rotation, the loudspeaker and boom arm wobbled as a torsional pendulum. After waiting sufficient time for the wobbling to dampen out, a new 30 s recording begins. This process was

repeated until 360 ^{o} of data had acquired per microphone radius. Since 0^{o} and 360^{o} were both measured, each radius resulted in 73, 30 s measurements. The FRFs of both angles were averaged together to represent that location resulting in 72 discrete locations and FRFs.

Full rotation measurements were taken at ten different radii in the azimuthal plane ranging from 0 ft to 8 ft in 1 ft increments. An additional measurement was taken at 8 ft 8 in, the maximum radial measurement that could be taken in the anechoic chamber before the microphone bumped into the wall wedges.

Chapter 3

Results

In a perfect free-field environment, the 72 FRFs for a given radius should be identical. Any differences in the FRFs can be attributed to nonanechoic effects in the chamber. To determine the extent of the differences in the FRFs, a frequency-dependent standard deviation for the various angles of each measurement radius was computed as suggested by Bodon [8]:

$$\sigma_n(f) = \sqrt{\frac{1}{N}\sum_{i=1}^{N}\left[\left|H_{n,i}(f)\right| - \mu_n(f)\right]^2}\ , \tag{1}$$

where

$$\mu_n(f) = \frac{1}{N}\sum_{i=1}^{N}\left|H_{n,i}(f)\right|\ , \tag{2}$$

N is the number of recordings per radius (72 in this case), i is the angular index, n is the radial index, and $\left|H_{n,i}(f)\right|$ is the i^{th} frequency response function for the n^{th} radius. Narrowband frequency-dependent standard deviations are plotted in Fig. 4 for all ten radial measurements.

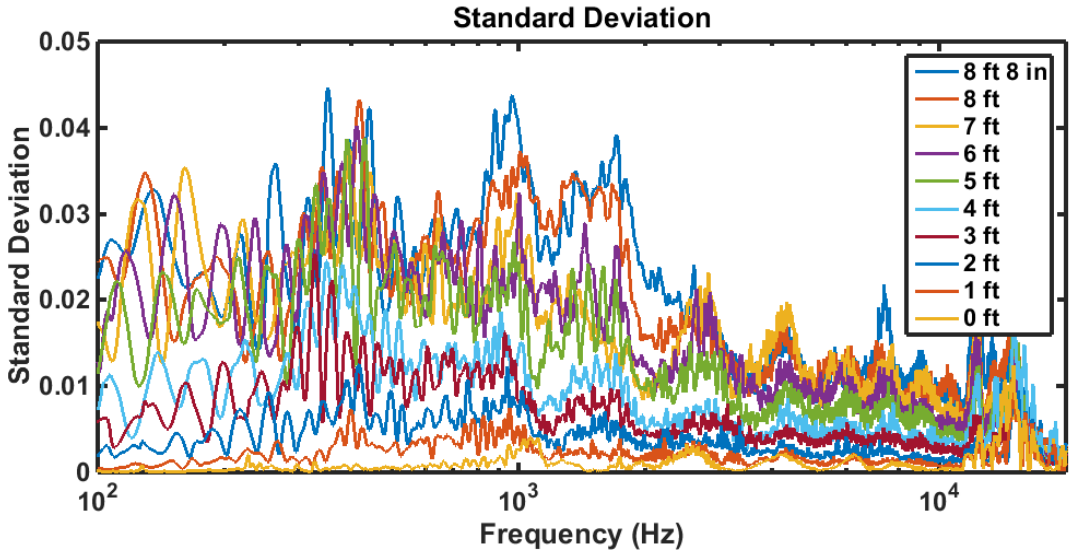

Figure 4. Standard deviations of ten radial measurements using 1 Hz bin width. Standard deviations were calculated from the 72 measurements in 5° increments at each radius.

To better understand the physical significance of these plots, an equivalent standard deviation level on a decibel scale was necessary. This was accomplished by computing the level variation range from the average by

$$\sigma_{dB_{diff}\,n}(f) = 2\,\{20\log[m_\sigma\sigma_n(f) + \mu_n(f)] - 20\log[\mu_n(f)]\}, \tag{3}$$

where m_σ is the standard deviation number used. Assuming a Gaussian distribution of the data, a standard deviation number of 3 includes 99.7% of the data. The subtracted logarithmic terms are multiplied by 2 in order to account for both the data above and below the mean FRF value, $\mu_n(f)$. The standard deviation difference level $\sigma_{dB_{diff}\,n}(f)$ represents the approximate sound pressure level difference between the maximum response of a given radial measurement to the minimum response. Simplification of Eq. (3) yields

$$\sigma_{dB_{diff}\,n}(f) = 40\log\left[\frac{m_\sigma\sigma_n(f) + \mu_n(f)}{\mu_n(f)}\right]. \tag{4}$$

Figure 5 shows the standard deviation difference in dB as calculated using this expression. A similar plot is shown in Fig. 6 with third-octave bins that effectively smooth the data.

In order to better visualize the extent of the standard deviations in the chamber, a surface plot of the FRF magnitudes is included in Fig. 7. Interpolated data points were generated at every degree angle and 3 inch radius in order to smooth the plot. The FRF magnitudes were normalized to each radii's average value at a given frequency. The loudspeaker is located at the center of the plot and each microphone recording corresponds to a point on the surface plot. The surface plot shows certain areas with a high response (areas that are more yellow) and low response (areas that are more blue). In an ideal free-field environment, this plot would be perfectly flat at 0 dB, with no spatial dependence of response.

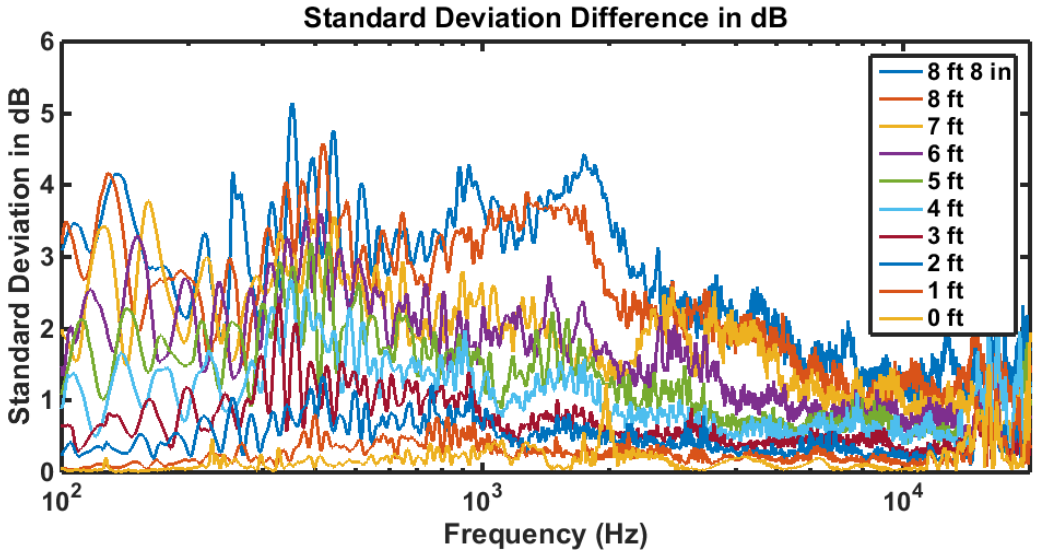

Figure 5. Standard deviation difference of ten radial measurements using 1 Hz bin width in dB. Standard deviations were calculated from the 72 measurements in 5° increments at each radius.

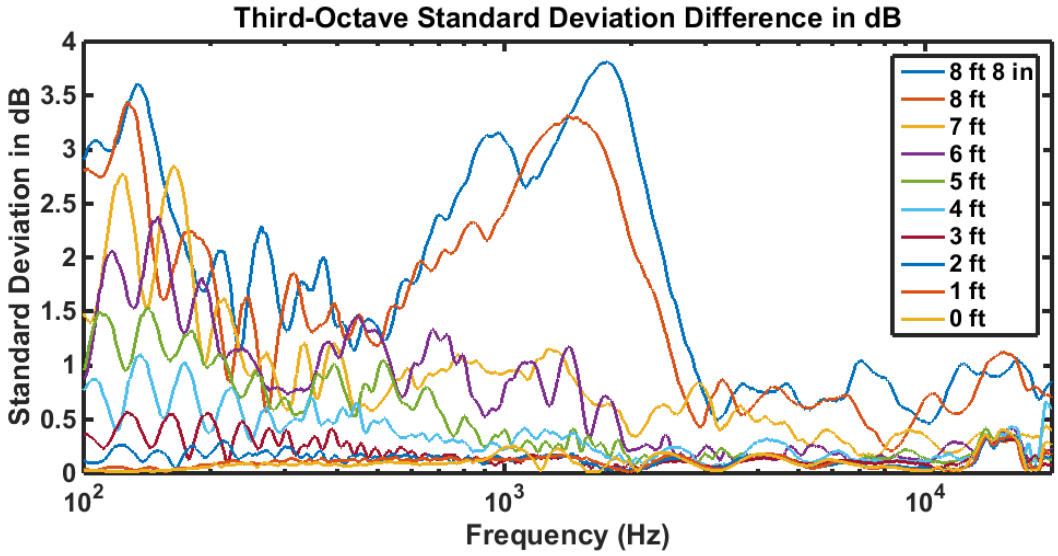

Figure 6. Standard deviation difference of ten radial measurements using proportional third octave bands of the power spectral density in dB. Standard deviations were calculated from the 72 measurements in 5° increments at each radius.

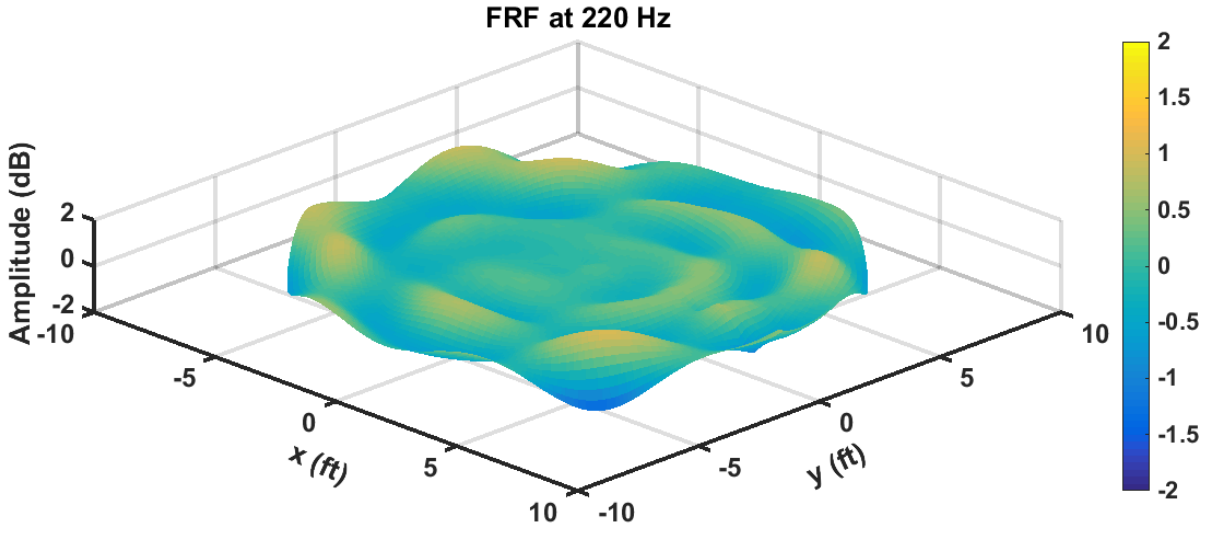

Figure 7. Frequency response function surface plot taken in the transverse plane at 220 Hz with a 1 Hz bin width. Center of the plot represents the loudspeaker location. Radial distances away from center represent microphone recording locations. Interpolated points are included at each degree angle and 3 inch radius.

Chapter 4

Analysis

4.1 Standard Deviation and Radius

Figure 5 shows a maximum of standard deviation difference of about 5 dB at 350 Hz for the 8 ft 8 in measurements. This is a surprisingly large difference considering that 350 Hz is within the anechoic range of the chamber. Both this figure and Fig. 6 show a trend of increasing standard deviation with increasing distance from the source, as would be expected if nonanechoic effects are present. Near the loudspeaker, the field is dominated by the direct sound. Farther from the loudspeaker, any reflected sound from the chamber walls has a more significant contribution to the field.

To better illustrate the trend of increasing standard deviation with increasing distance, an average of each standard deviation difference was taken across the specified anechoic frequency range of the anechoic chamber (80 Hz – 20 kHz). Figure 8 shows the result for each radial distance.

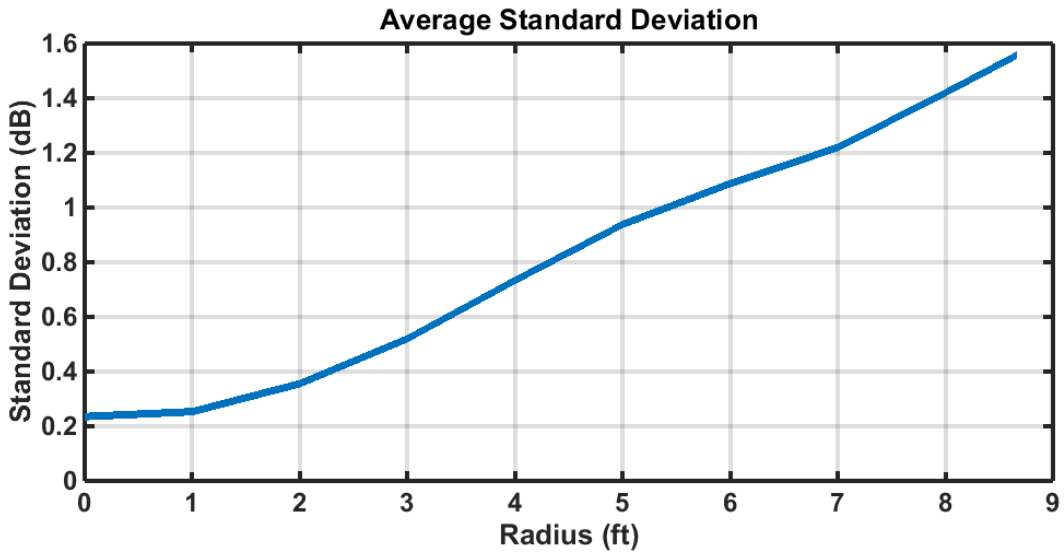

Figure 8. The average standard deviation difference in dB for each radial measurement distance in the transverse plane with 1 Hz bin width.

4.2 Low-Frequency Cutoff Frequency

Measurements are expected to have a high standard deviation for frequencies below the low-frequency cutoff of the anechoic chamber. When viewing the standard deviation difference of the 10 radial measurements at lower frequencies (see Fig. 9), an interesting result is apparent. Each plot has a region of low standard deviation followed by a steep rise in standard deviation at lower frequencies. When viewing the 8 ft 8 in case, we see that the cutoff frequency of low standard deviation (as shown by the star) corresponds to about 80 Hz. This is the currently understood low-frequency cutoff of the BYU anechoic chamber. At 8 ft, we see that the cutoff frequency is approximately 75 Hz, and so on for the other radial measurement distances.

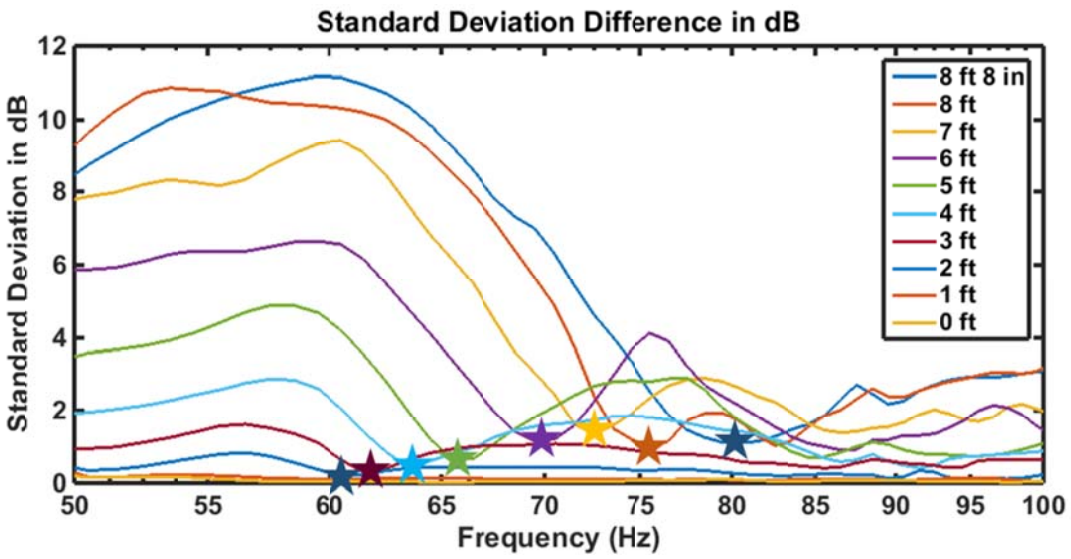

Figure 9. Low-frequency standard deviation difference of ten radial measurements using 1 Hz bin width. Stars represent the low frequency cut-off for the given radius.

There is a notable trend for cutoff frequencies as the radii decrease. Since low standard deviation corresponds to a well-performing anechoic chamber, it is concluded that the low-frequency cutoff of the chamber actually depends on the distance from a source. Figure 10 depicts the cutoff frequencies as a function of radial distance.

Researchers can greatly benefit from this information. Since the established low-frequency cut-off of the BYU chamber is 80 Hz, researchers typically limit their studies to frequencies above 80 Hz. However, with this finding, they can increase the low-frequency range of their measurements by taking measurements closer to a source. For example, by placing a microphone 2 ft away from a source, a researcher can extend his or her studies down to 60 Hz.

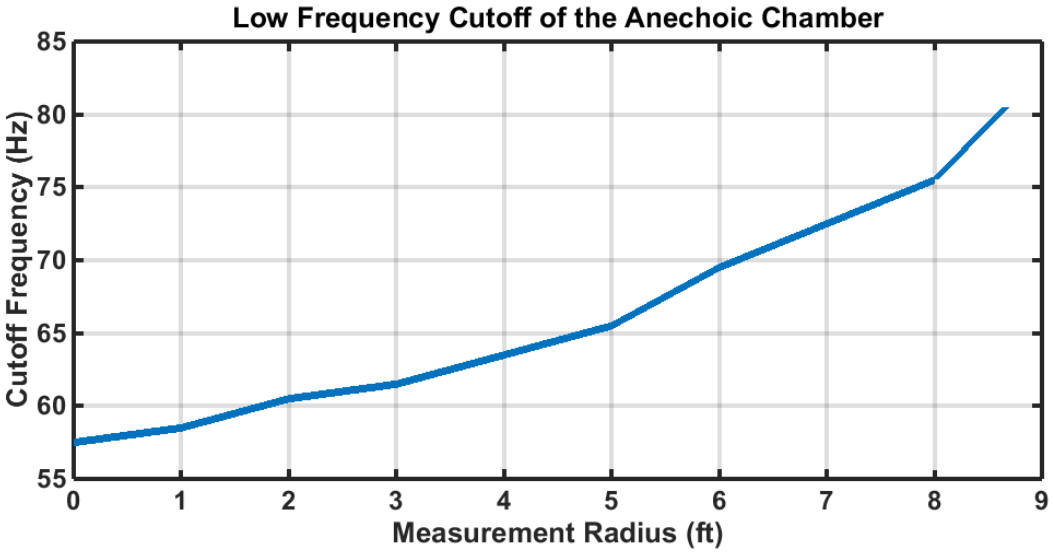

Figure 10. Low-frequency cutoff of the anechoic chamber as a function of measurement radius.

4.3 Validation

It is possible that noise and other imperfections in the loudspeaker, microphone, or other devices in the signal acquisition system could artificially cause variances in the recording response. In order to ensure that the variances could be attributed to the chamber, a simple experiment was performed. The constant-excitation device was used to take a full set of measurements (73, with 30 s of Gaussian noise, at the ten radial distances) but without incorporating any rotation. This meant that the system remained stationary during all measurements. This effectively eliminated the chamber as a variable that could cause variance in the recorded responses. Identical processing techniques were used to compute the standard deviations and FRF plots.

Figure 11 shows the standard deviation difference in dB for the no-rotation experiment on the same scale as used for Fig. 5. The standard deviations are well below 0.5 dB for the

majority of frequencies. By comparing the figures, it becomes clear that the recording location in the chamber does have a significant effect on anechoic chamber measurements.

The slight increase in standard deviation near 15 kHz in Fig. 11 is present at all radii. This corresponds to the drop in the frequency response and coherence of the loudspeaker as seen in Figs. 12 and 13. A lower loudspeaker response reduces the signal-to-noise ratio of the FRF. This allows uncorrelated noise in the chamber or electronics to corrupt the data, causing an increase in standard deviation.

Additionally, FRF surface plots were produced to visualize the differences between rotation and no-rotation measurements. Figure 14 shows comparisons for three frequencies, with rotation measurements to the left and no-rotation (or control) measurements to the right. Note that the no-rotation measurements were plotted as if a rotation was implemented for comparison. The no-rotation FRFs are very flat, showing that there is very little variation between measurements when the constant-excitation device was not rotated. Again, it is clear that the recording location in the anechoic chamber can have a significant effect on anechoic chamber measurements.

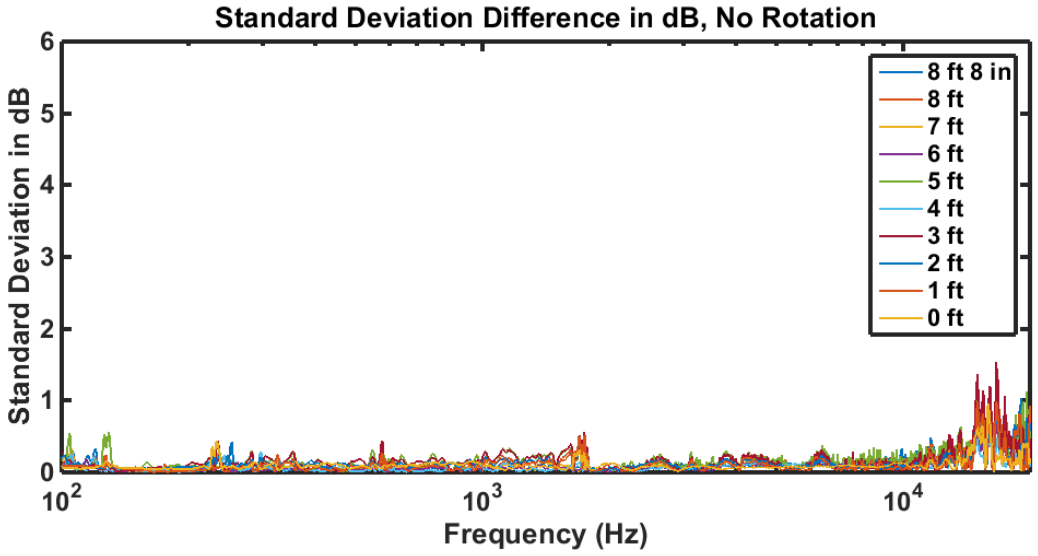

Figure 11. Standard deviation difference of ten radial measurements using 1 Hz bin width. No rotation was implemented in these measurements.

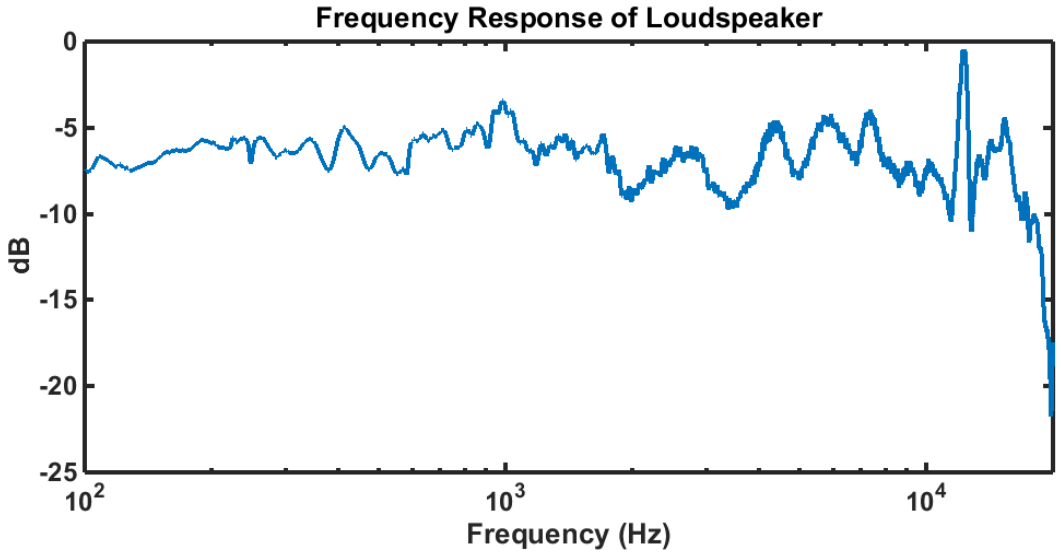

Figure 12. Measured on-axis frequency response of the PreSonus Sceptre S6 coaxial loudspeaker using 1 Hz bin width.

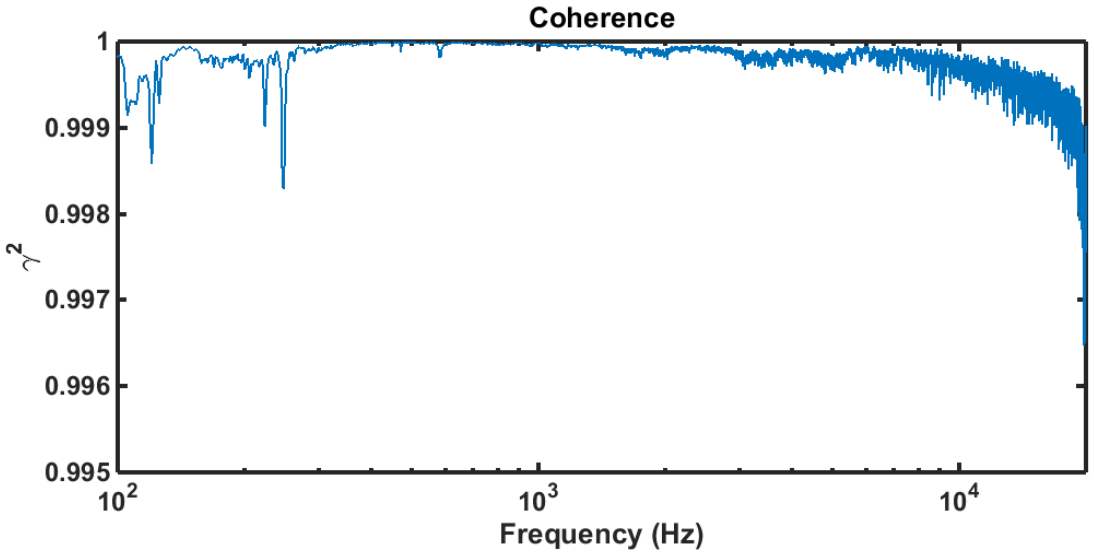

Figure 13. Measured on-axis coherence of the PreSonus Sceptre S6 coaxial loudspeaker shown in Fig. 12 using 1 Hz bin width.

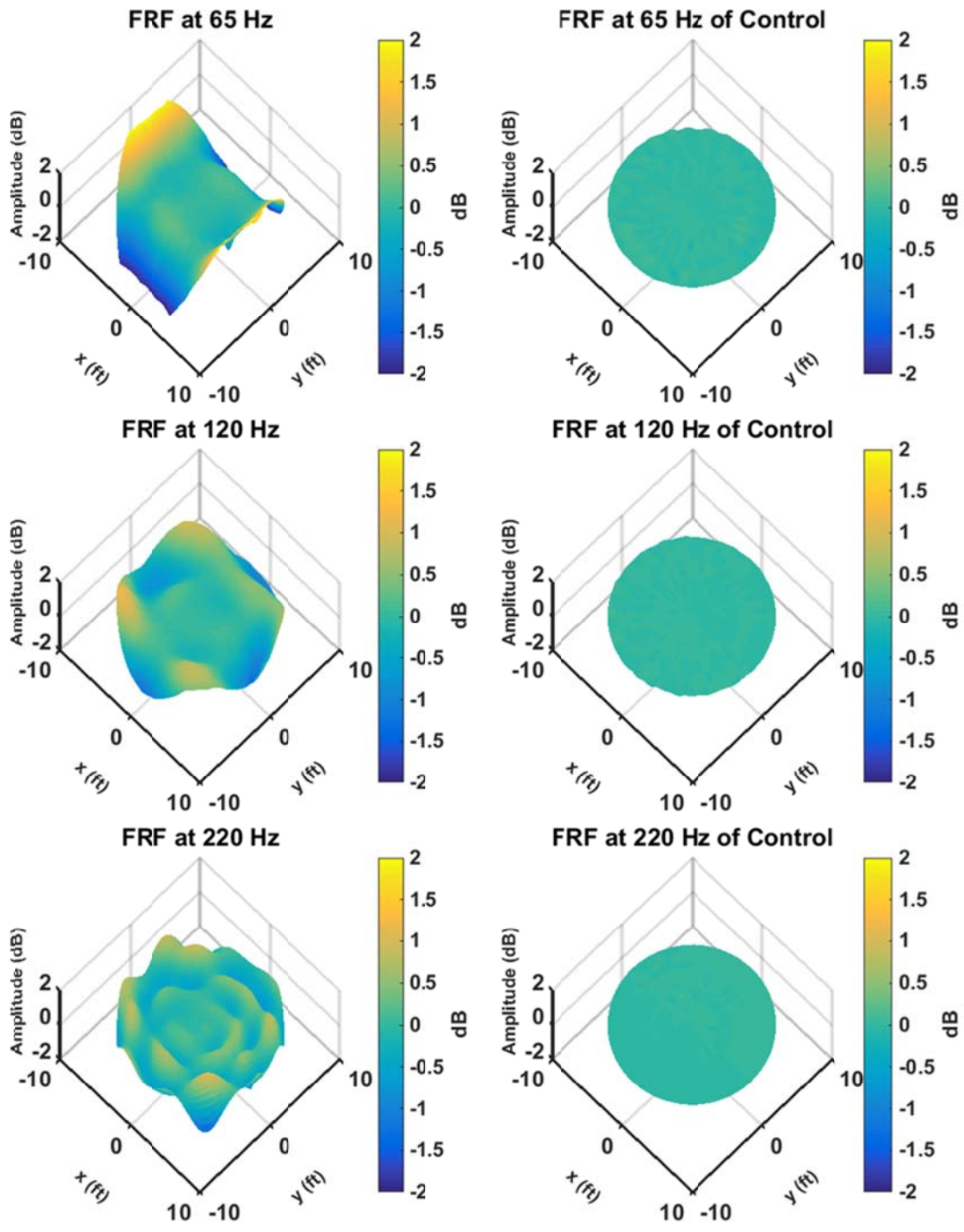

Figure 14. Comparisons of FRF surface plots between rotation (left column) and no-rotation included (right column) measurements.

Chapter 5

Conclusions

The anechoic chamber has a greater effect on sound measurements than many researchers realize. A standard deviation difference of up to 5 dB was shown to be a potentially significant cause of error for fixed-radius, multiple-angle measurements, such as directivity and sound power measurements. Standard deviation and FRF surface plots are useful tools for understanding the extent of nonideal effects of anechoic chambers.

Researchers can use the methods outlined in this report to characterize nonanechoic effects in other chambers around the world. The resulting understanding of nonanechoic effects on measurements will lead to more reliable and repeatable sound measurements in the future.

Future research can be done to extend the methods for use in improved anechoic chamber qualification standards. The approach will more accurately characterize anechoic chambers for use in fixed-radius, multiple-angle measurements than the current ISO 3745 standard. It will eventually lead to higher-quality anechoic chambers and more reliable acoustical measurements.

References

[1] ISO 3745:2012: Acoustics-Determination of sound power levels of noise sources – Precision methods for anechoic and semi-anechoic rooms (International Organization for Standardization, Geneva, Switzerland).

[2] K. A. Cunefare, J. Badertscher, and V. Wittstock, "On the qualification of anechoic chambers; Issues related to signals and bandwidth," J. Acoust. Soc. Am. 120, 820-829 (2006).

[3] K. A. Cunefare, V. B. Biesel, J. Tran, R. Rye, A. Graf, M. Holdhusen, and A. M. Albanese, "Anechoic chamber qualification: Traverse method, inverse square law analysis method, and nature of test signal," J. Acoust. Soc. Am. 113, 881-892 (2003).

[4] R. J. Fridrich, "Is This Room Anechoic? A New Anechoic Room Qualification Standard May Be Needed for Impulsive Sound Quality Tests," SAE International Technical Paper No. 2007-01-2217 (2007).

[5] P. Saussus and K. A. Cunefare, "High-frequency monopole sound source for anechoic chamber qualification," J. Acoust. Soc. Am. 113, 2219-2219 (2003).

[6] M. P. M. Luykx, "Reflections in anechoic rooms," Proc. Inter-noise and Noise-Con Congress, 2534-2537 (2001).

[7] N. Olsen, "Acoustic Properties of Anechoic Chamber," J. Acoust. Soc. Am. 33, 767-770 (1961).

[8] K. J. Bodon, "Development, Evaluation, and Validation of a High-Resolution Directivity Measurement System for Played Musical Instruments," M.S. thesis, Brigham Young University, Provo, Utah (2016). Available online at <http://scholarsarchive.byu.edu/etd/5653/> (Last viewed April 23, 2016).